Comparison of Radiation Transport Codes, HZETRN, HETC and FLUKA, Using the 1956 Webber SPE Spectrum

John H. Heinbockel and Tony C. Slaba
Old Dominion University, Norfolk, Virginia

Steve R. Blattnig and Ram K. Tripathi
Langley Research Center, Hampton, Virginia

Lawrence W. Townsend, Thomas Handler, and Tony A. Gabriel
University of Tennessee, Knoxville, Tennessee

Lawrence S. Pinsky and Brandon Reddell
University of Houston, Houston, Texas

Martha S. Clowdsley, Robert C. Singleterry, and John W. Norbury
Langley Research Center, Hampton, Virginia

Francis F. Badavi
Christopher Newport University, Newport News, Virginia

Sukesh K. Aghara
Prairie View A & M University, Prairie View, Texas

January 2009

Contents

List of Figures

Abstract

Protection of astronauts and instrumentation from galactic cosmic rays (GCR) and solar particle events (SPE) in the harsh environment of space is of prime importance in the design of personal shielding, spacecraft, and mission planning. Early entry of radiation constraints into the design process enables optimal shielding strategies, but demands efficient and accurate tools that can be used by design engineers in every phase of an evolving space project. The radiation transport code, HZETRN, is an efficient tool for analyzing the shielding effectiveness of materials exposed to space radiation. A systematic effort of verification and validation is now underway to quantify the accuracy of HZETRN and elucidate any weaknesses. In this paper, HZETRN is compared to the Monte Carlo codes HETC-HEDS and FLUKA, for a shield/target configuration comprised of a 20 g/cm^2 Aluminum slab in front of a 30 g/cm^2 slab of water exposed to the February 1956 SPE, as modeled by the Webber spectrum. Neutron and proton fluence spectra, as well as dose and dose equivalent values, are compared at various depths in the water target. Fluence spectra produced by HZETRN are also given for ^2H, ^3H, ^3He and ^4He ions at various depths in the water target. This study shows that there are many regions where HZETRN agrees with both HETC-HEDS and FLUKA for this shield/target configuration and the SPE environment. However, there are also regions where there are appreciable differences between the three computer codes.

1 Introduction

One of the objectives of the NASA Strategic Plan for the human exploration of space is to develop space radiation protection for both astronauts and instrumentation [1]. An important step in achieving this goal is to provide design engineers with an efficient radiation transport code with an estimate of accuracy under a variety of design scenarios. Such a code can then be used in every phase of vehicle, shelter, and mission design to enable optimal shielding strategies that satisfy radiation constraints and objectives.

The HZETRN (High charge(Z) and Energy TRaNsport) computer code has been used for radiation analysis under a variety of shielding conditions in solar particle event (SPE), galactic cosmic ray (GCR), and low earth orbit (LEO) environments. While the code has endured several rounds of verification and validation in these environments [2, 3, 4], most of the comparisons focused on integrated quantities, such as dose or dose equivalent, and individual ion fluences were not examined in detail. Though dose or dose equivalent were generally viewed as sufficient tests for evaluating code accuracy, recent interest in fluence based approaches to radiation risk assessment demand a higher degree of accuracy from

the code [5]. This, along with recent improvements to some of the underlying transport models and numerical procedures [6, 7, 8], provides an opportunity to expose HZETRN to another round of verification and validation benchmarks.

In this paper, a 20 g/cm^2 Aluminum slab shield and a 30 g/cm^2 water slab target exposed to the February 1956 SPE spectrum, as modeled by Webber [9, 10] is used as a benchmark case to compare HZETRN to the Monte Carlo codes HETC - HEDS (High Energy Transport Code - Human Exploration and Development of Space) [11, 12] and FLUKA [13, 14]. The 20 g/cm^2 Aluminum slab is a common thickness for space vehicles and the 30 g/cm^2 water slab simulates body tissue.

While HZETRN has historically transported all particles in the straight ahead direction, recent efforts have provided a bi-directional neutron transport model that is fully coupled to the existing transport algorithm. References [6, 8, 15, 16] provide a complete description of the straight ahead transport procedure, and a brief description of the the bi-directional neutron transport model and coupling mechanisms used by HZETRN is provided. An overview of the Monte Carlo codes is also given with suitable references to provide more detailed information. Forward and backward neutron fluences and proton fluences are generated using all three codes and results are compared at various depths in the water target. Dose and dose equivalent comparisons between HZETRN, HETC-HEDS and FLUKA are given. Since HZETRN also transports ^{2}H, ^{3}H, ^{3}He and ^{4}He for any SPE environment, these fluence spectra are also presented.

2   HZETRN

HZETRN is a suite of codes containing a numerical solution for the Boltzmann transport equation with the continuous slowing down and straight ahead approximations. The code has evolved over a 25 year period from the work of John W. Wilson and co-workers at the NASA Langley Research Center [15]. Several corrections and modifications have been added in recent years. A more robust method for handling neutron elastic interactions has been included [6], and a bi-directional neutron transport model has been fully coupled into the code. Light ion (A < 5) cross sections have been extracted to allow greater computational flexibility and efficiency. These cross sections were previously imbedded in the code.

The Boltzmann transport equation, with the continuous slowing down and straight ahead approximations, is given by [15]

$$B[\phi_j(x,E)] = \sum_k \int_E \sigma_{jk}(E,E')\phi_k(x,E')\,dE' \, , \tag{1}$$

where

$$B[\phi_j(x,E)] \equiv \left[\frac{\partial}{\partial x} - \frac{1}{A_j} \frac{\partial}{\partial E} S_j(E) + \sigma_j(E) \right] \phi_j(x,E) \qquad (2)$$

is a differential operator. Here, $\phi_j(x,E)$ denotes the fluence of type j particles at depth x having kinetic energy E, A_j is the atomic mass of a type j particle, $S_j(E)$ is the stopping power of the jth particle with kinetic energy E, $\sigma_j(E)$ is the macroscopic cross section, and $\sigma_{jk}(E, E')$ are the production cross sections for interactions where a type k particle with energy E' produces a type j particle with kinetic energy E.

The following are some notes concerning the calculation of the numerical solutions to equation (1). For heavy ions ($A > 4$), it is noted that projectile fragments, after leaving a collision event, will have energy very near that of the projectile. Therefore, spectral distributions in the production cross sections become very narrow and allow for easy evaluation of the source integral on the right hand side of equation (1) [15]. Further, target fragments created by heavy ion projectiles are not explicitly transported due to their low range (they are accounted for in dose calculations) and so the summation in equation (1) is taken over k such that $A_k > A_j$ [15, 17]. For light ions, neither of these approximations is valid. The broad energy distribution in collision events prohibits simplification of the source integral, and both projectile and target fragments are transported, so that the summation over projectile particle type must be taken over all light ions [17]. Since this paper deals with the February 1956 Webber SPE spectrum, for which there is a negligible heavy ion component, no more will be said about heavy ion transport in HZETRN.

Wilson et al. have developed an accurate marching algorithm to transport light ions in the straight ahead direction [8, 15, 16]. The formulation and implementation of the procedure has not changed much in recent years, but Slaba et al. [6] have provided a more robust method of handling low energy neutron elastic interactions, and light ion cross sections have been successfully extracted from the code to allow greater computational efficiency and most importantly, the ability to interchange cross section models and databases as necessary to carry out future verification and validation efforts.

The most notable modification to the HZETRN code came in recent years with the culmination of several works [18] - [24]. Slaba et al. [7] have developed an efficient and accurate bi-directional neutron transport model that is completely coupled into the existing light ion transport procedure. The fluence ϕ_j is split into a straight ahead (sa) and isotropic (iso) component by writing

$$\phi_j(x,E) = \phi_j^{iso}(x,E) + \phi_j^{sa}(x,E) \ , \qquad (3)$$

where it has been demonstrated that the straight ahead component is associated with higher energy primary or cascade projectile fragments produced in nearly the same direction of the projectile, and the isotropic component is associated with particles ejected

from excited projectile fragments or evaporation. Similarly, the neutron nuclear reactive production cross section is split into straight ahead and isotropic components as

$$\sigma_{nk}(E, E') = \sigma_{nk}^{r,iso}(E, E') + \sigma_{nk}^{r,sa}(E, E') , \qquad (4)$$

where the superscript r denotes the nuclear reactive component of the neutron production cross section and the subscript n denotes neutrons. The straight ahead component of the particle fluences are first computed by solving

$$B[\phi_j^{sa}] = \sum_k \int_E \kappa_{jk}(E, E')\phi_k^{sa}(x, E')\, dE' , \qquad (5)$$

using the light ion marching algorithm developed by Wilson et al. [8, 15, 16], with $\kappa_{jk}(E, E')$ given by the piecewise definition

$$\kappa_{jk}(E, E') = \begin{cases} \sigma_{nk}^{r,sa}(E, E'), & j = n \\ \sigma_{jk}(E, E'), & j \neq n . \end{cases} \qquad (6)$$

The isotropic neutron source term,

$$\eta_n(x, E) = \sum_k \int_E \sigma_{nk}^{r,iso}(E, E')\phi_k^{sa}(x, E')\, dE' , \qquad (7)$$

is then calculated, and the isotropic neutron fluence ϕ_n^{iso} is decomposed into a forward and backward component by writing

$$\phi_n^{iso}(x, E) = \phi_n^f(x, E) + \phi_n^b(x, E) . \qquad (8)$$

A collocation method [7, 23, 24] is finally used to obtain a Neumann series solution to the directionally coupled neutron transport model,

$$\left[\frac{\partial}{\partial x} + \sigma_n(E)\right] \phi_n^f(x, E) = \int_E \sigma_n^{(+)}n(E, E')\phi_n^f(x, E')\, dE'$$
$$+ \int_E \sigma_n^{(-)}n(E, E')\phi_n^b(x, E')\, dE' + \frac{1}{2}\eta_n(x, E) , \qquad (9)$$

$$\left[-\frac{\partial}{\partial x} + \sigma_n(E)\right] \phi_n^b(x, E) = \int_E \sigma_{nn}^{(+)}(E, E')\phi_n^b(x, E')\, dE'$$
$$+ \int_E \sigma_{nn}^{(-)}(E, E')\phi_n^f(x, E')\, dE' + \frac{1}{2}\eta_n(x, E) . \qquad (10)$$

The production cross section, $\sigma_{nn}^{(+)}(E, E')$, represents nuclear reactive and elastic interactions, in which the scattering angle between the pre - collision and post-collision neutron is between $[0, \pi/2]$ with respect to the propagation direction of the pre-collision neutron.

Conversely, $\sigma_{nn}^{(-)}(E, E')$ represents nuclear reactive and elastic interactions in which the scattering angle between the pre-collision and post-collision neutron is between $[\pi/2, \pi]$ with respect to the propagation direction of the pre-collision neutron. This implies that the second integral on the right hand side of equation (9) represents forward propagating neutrons produced by backward propagating neutrons, and the second integral on the right hand side of equation (10) represents backward propagating neutrons produced by forward propagating neutrons. In order to couple this bi-directional neutron solution back into the light ion transport procedure, the isotropic light ion source terms,

$$\eta_j^{iso}(x, E) = \int_E \sigma_{jn}(E, E')\phi_n^{iso}(x, E') \, dE' \,, \tag{11}$$

are calculated, and the isotropic component of the light ion fluences are obtained by computing

$$\begin{aligned} \phi_j^{iso}(x, E) &= \frac{P_j(E_\gamma)S_j(E_\gamma)}{P_j(E)S_j(E)} \, \phi_j^{iso}(x, E_\gamma) \\ &+ \int_E^{E_\gamma} \frac{A_j P_j(E')}{P_j(E)S_j(E)} \, \eta_j(x + R_j(E) - R_j(E'), E') \, dE' \,, \end{aligned} \tag{12}$$

where $R_j(E)$ is given by the range-energy relation,

$$R_j(E) = A_j \int_0^E \frac{dE'}{S_j(E')} \,, \tag{13}$$

and $P_j(E)$ is the nuclear survival probability defined by

$$P_j(E) = \exp\left[-A_j \int_0^E \frac{\sigma_j(E')}{S_j(E')} \, dE' \right] \,, \tag{14}$$

with the residual energy given by $E_\gamma = R_j^{-1}[x + R_j(E)]$. More detailed information regarding these transport models and numerical implementations can be found in the references [7, 18].

3 Monte Carlo Codes

The term, Monte Carlo, is used to describe a random walk algorithm that simulates an event and then performs a statistical analysis of the results. Monte Carlo techniques are typically constructed whenever there is a high dimensional integral equation that cannot be solved either analytically or numerically with deterministic methods. To reduce the computing time involved in Monte Carlo techniques, variance reduction is often employed. A brief description of Monte Carlo methods applied to radiation transport can be found

in reference [25]. In this paper, the results from the two Monte Carlo codes HETC-HEDS [11, 12] and FLUKA [13, 14], are used to verify the results calculated by the deterministic code HZETRN. The following is a brief description of HETC-HEDS and FLUKA used in this study.

3.1   HETC-HEDS

The HETC-HEDS computer code is a Monte Carlo based solution method designed specifically for solving space radiation problems, [11, 12] associated with secondary particle fields produced by space radiation interacting with shielding and equipment. It is a three dimensional generalized radiation transport code capable of handling and analyzing radiation fields which affect critical body organs of astronauts such as bone marrow and the central nervous system.

HETC-HEDS can be applied to a wide range of particle species and energies. It contains a heavy ion collision event generator capable of tracking nuclear interactions and performing statistical analysis of the data. It simulates particle interactions by using a pseudo random number generator, along with the appropriate physics, to follow trajectories of primary particles and all secondary particles involved in the nuclear collision of galactic cosmic rays and solar event particles interacting with shielding material, biological organisms, and electronic equipment.

The geometry input is simple combinatorial volumes. The cross sections are generated internally, as part of the software. The HETC-HEDS computer code employs all particles of interest for space radiation. In particular, HETC-HEDS considers interactions of protons, neutrons, π^+, π^-, μ^+, μ^-, light ions and heavy ions. These particles can be arbitrarily assigned position, angle, and energy throughout a spatial boundary. In essence, this Monte Carlo code follows each particle in a cascade until it undergoes a nuclear collision, absorption, decays, escapes from the spatial boundary, or is eliminated by crossing a domain variable cutoff. The nuclear reactions and processes are accounted for by using appropriate physical models to handle such things as energy losses, range straggling, Coulomb scattering, etc. Both elastic and nonelastic collisions are considered using energy and nucleon conservation principles.

This Monte Carlo package has no capability to determine when the solution method has converged on the answer sought within some confidence interval. It does provide the means for predicting the interaction product yields, production angles, and energies using nuclear models for transport processes. It has been extensively used for code verification, bench marking and testing against available laboratory beam data.

3.2   FLUKA

The FLUKA computer code is a general purpose Monte Carlo computer program used for calculating particle transport and interaction with various materials. It has the ability

to transport and interact all elementary hadrons, light and heavy ions, and electrons and photons over an energy range which extends up to 10^4 TeV for all particles, and down to thermal energies for neutrons [13, 14]. The code has built in capabilities for scoring particle fluences, yields, and energy deposition over arbitrary three dimensional meshes, both on an event by event basis or averaged over a large number of histories.

This code has been extensively benchmarked against available accelerator and cosmic ray experimental data, at beam energies as low as a few MeV and as large as cosmic ray energies. These spectra can be modulated within FLUKA according to an arbitrary solar activity modulation parameter, or, for dates in the past, using the actual solar activity as measured by ground based neutron counters.

Three different Earth magnetic field descriptions of increasing complexity can be used. Geomagnetic cut offs can be input or calculated. Spectra representative of some of the largest solar particle events are also pre-built into the code. In addition to galactic cosmic rays and solar particle events, this code has a wide range of particle physics application areas where it can be employed. It has demonstrated that it can simulate nuclear interactions and events with great accuracy in several fields, including particle physics, dosimetry, accelerator driven nuclear systems, detector characterization, aircraft crew dosimetry, shielding, and hadron therapy. The code can simulate interactions involving over sixty different particle types and can handle complex geometries. The geometry input has two levels: the basic one consisting of combinatorial volumes, and a second level, the so called "lattice" level, which allows repetition and arbitrary spatial placement of the complex object defined at the first level. It also allows for a voxel (a volume element, representing a value on a regular grid in three dimensional space) input stream which can be combined with a standard combinatorial geometry input, allowing for example to embed a detailed voxel description of a human being, such as derived from a computed tomography (CT) scan, within an arbitrarily complicated spacecraft shape.

The nuclear models and associated cross sections are hard coded into the software for all particles and energies, with the exception of neutrons below 20 MeV, where a 260 neutron group library obtained from standard international evaluated data files is used. The FLUKA computer code contains many variance reduction algorithms and covers all particles of interest for space radiation research. For most applications, the FLUKA package requires no additional programming.

The code provides a large variety of statistical techniques for analyzing nuclear interactions. The offline analysis tools provided with the code enable one to perform simple statistical analysis of the results. The code comes with a powerful Graphical User Interface, FLAIR, which allows an easy setup of the input stream and the geometry. It also provides user friendly tools for running the code and analyzing and plotting the results.

4 Results and Discussions

The 1956 Webber differential and integral SPE spectrum, with 100 MV rigidity, is illustrated in figure 1. The Webber spectrum is given by

$$
\begin{aligned}
\frac{d\phi}{dE} &= 10^7 \frac{E+938}{\sqrt{E(E+1876)}} \exp\left\{\left[239.1 - \sqrt{E(E+1876)}\right]/100\right\} \quad \frac{\#\text{particles}}{\text{cm}^2\,\text{MeV}}, \\
\phi &= 10^9 \exp\left\{\left[239.1 - \sqrt{E(E+1876)}\right]/100\right\} \quad\quad\quad \frac{\#\text{particles}}{\text{cm}^2},
\end{aligned}
\tag{15}
$$

and is exclusively a proton spectrum [9, 10].

Figures 3 - 19 present selected results generated by the three radiation codes used to transport the February, 1956 Webber SPE through a 20 g/cm^2 Aluminum slab shield and a 30 g/cm^2 water slab target. Figures 20 - 23 illustrate ^{2}H, ^{3}H, ^{3}He and ^{4}He fluences predicted by HZETRN. These four light ions along with neutron and protons are the six light ions transported by HZETRN for SPE environments. They have been included in this paper to give a complete picture of the particles used by HZETRN to calculate dosimetric quantities for SPE environments.

Observe that in many sections of the graphs presented, the data from all three computer codes are overlapping and consequently one cannot distinguish some of the markers. A cursory examination of the results presented in figures 3 - 19 allows one to conclude that there is a good qualitative agreement between the transport codes in many regions. However, there are some regions where there are significant differences between the codes, and the following discussion will address these issues.

For a quantitative assessment of the dose and dose equivalent curves, we select a root mean square analysis of the data. Recall that the root mean square between data sets $\{Y_i\}$ and $\{y_i\}$ for $i = 1, \ldots, N$ is given by

$$
\text{RMS} = \sqrt{\frac{\sum_{i=1}^{N}(Y_i - y_i)^2}{N}},
\tag{16}
$$

where N is the number of ordinates in the data sets with the abscissa values being the same for each data set. We make a RMS comparison between the HZETRN, FLUKA and HETC-HEDS data sets and obtain

$$
\begin{aligned}
\text{RMS}_{\text{Dose}_{(\text{HZETRN}-\text{HETC})}} &= 0.176 \text{ cGy}, \\
\text{RMS}_{\text{Dose}_{(\text{HZETRN}-\text{FLUKA})}} &= 0.212 \text{ cGy}, \\
\text{RMS}_{\text{Dose}_{(\text{FLUKA}-\text{HETC})}} &= 0.043 \text{ cGy}.
\end{aligned}
\tag{17}
$$

An examination of the dose equivalent curves in figure 4 shows there is a significant difference between the calculated results. We again use a root mean square analysis for a

quantitative measure of agreement between the data sets and obtain the value

$$\text{RMS}_{\text{DoseEq(HZETRN-HETC)}} = 1.085 \text{ cSv} ,$$
$$\text{RMS}_{\text{DoseEq(HZETRN-FLUKA)}} = 0.184 \text{ cSv} ,$$
$$\text{RMS}_{\text{DoseEq(FLUKA-HETC)}} = 1.008 \text{ cSv} . \tag{18}$$

Note that a small RMS value implies better overall agreement between the data sets. For the dose curves, there is good agreement between FLUKA and HETC-HEDS. For the dose equivalent curves, the best agreement is between HZETRN and FLUKA. Both the HZETRN and FLUKA computer codes use the ICRP-60 standard for calculating dose and dose equivalent, while HETC-HEDS uses the ICRP-25 standard. It should also be emphasized that HZETRN does not transport certain particles such as pions, muons, positrons, electrons, and photons. These particles are used in calculating dose and dose equivalent by HETC-HEDS and FLUKA, but not HZETRN. The contribution of these particles to dose and dose equivalent values can be significant. Also, the HETC-HEDS uses the NCRP 132 [26] and 142 [27] conversion factors in combination with the DABL69 KERMA factors [28]. The HZETRN code does not use KERMA factors in the calculation of dose and dose equivalent. The number and type of particles used and the algorithm employed for calculating the dose and dose equivalent could account for the differences in the calculation of the dose and dose equivalent curves [25]. In calculation of the dose equivalent, the HZETRN code uses the lineal energy quality factor $Q(L)$ as defined in reference [29]

$$\begin{aligned} Q(L) &= \quad 1, & L < 10 \text{ keV}/\mu\text{m} , \\ Q(L) &= 0.32L - 2.2, & 10 \text{ keV}/\mu\text{m} \leq \text{L} \leq 100 \text{ keV}/\mu\text{m} , \\ Q(L) &= \quad 300L^{-0.5}, & L > 100 \text{ keV}/\mu\text{m} . \end{aligned} \tag{19}$$

where $L = LET$ represents the linear energy transfer. The graph of $Q(L)$ is illustrated in figure 2.

Comparisons of the dose and dose equivalent curves are illustrated in the figures 3 and 4. The low energy ($< 20\text{Mev}$) neutrons contribute to the dose equivalent next to only the primary source protons. HETC-HEDS used the older neutron conversion factors to convert from dose to dose equivalent. When the updated conversion factors are used, the total dose equivlent from HETC-HEDS increases by approximately a factor of 1.25. If this correction is applied to the data in figure 4, then the curve labeled "Corrected HETC-HEDS" results and one can see that the three curves are then in good agreement.

The forward, backward and total neutron fluence curves are illustrated in figures 5 through 15. The HZETRN and HETC-HEDS are in excellent agreement since the curves are essentially on top of one another over the energy range displayed. The FLUKA results are lower over the energy range $E < 100$ MeV. Also, note that the results from the Monte Carlo codes tend to oscillate over the low energy range. This can sometimes be due to

9

lack of convergence of the data, but this may or may not be the actual reason for the oscillations.

In figures 9 - 11, HZETRN is differing from both HETC-HEDS and FLUKA over the high energy range representation for the backward neutron fluence. This is probably due to the HZETRN forward-backward modeling putting too much emphasis on the backward component of the fluence. Another possibility for the differences is that the cross sections being used for the backward model need modification over this energy range. The reason for the backward neutron fluence differences will require further investigation of the HZETRN code. The HZETRN backward fluence does agree with HETC-HEDS results over the low energy range, with the FLUKA results being substantially lower. Note that at 30 g/cm^2 in the water target, there are no backward neutron fluences. Only outgoing, forward particles are allowed at this depth. Figures 12 - 15 show agreement of total neutron fluence for the three codes over the high energy range $E > 100$ MeV. Figures 12 - 15 show differences over the low energy range. The results from FLUKA are lower than those of HZETRN and HETC-HEDS. These figures also show differences between HZETRN and FLUKA in the total neutron fluence over the mid energy range.

The proton curves of figures 16 - 19 are essentially on top of one another, with FLUKA illustrating oscillations over the low energy range which can be caused by lack of convergence or upon the setting of the lower energy limit for the FLUKA code. Note that the computed fluence spectrum from HZETRN, which at low energies is in a quasi-equilibrium state [25], is divided by the stopping power of protons in tissue with a peak displayed around 0.1 MeV. This is similar to the classical Bragg peak as described in reference [25]. A similar type of statement can be made about the dips illustrated in figures 20 - 23.

Figures 20 - 23 are included to illustrate the light ion production produced by the HZETRN code. These values can serve as a HZETRN benchmark for any future comparison studies. Also, note that these results, together with the neutron and proton production, are major contributors used by HZETRN in the calculations of the dose and dose equivalent values.

Figure 24 is an enlargement of the energy range $1 \leq E \leq 100$ MeV for the total neutron fluence from figure 15. This graph is representative of the existing differences between the results produced by the three computer codes. This region is particularly important because this is where the quality factors undergo the most change, as illustrated in figure 2.

5   Conclusions

Selected curves have been presented from a comparison study where the transport codes HZETRN, HETC-HEDS and FLUKA each analyzed particle transport for a shield and target configuration of 20 g/cm^2 Aluminum slab in front of a 30 g/cm^2 water slab, which is exposed to the February 1956 SPE, as modeled by the Webber spectrum. The

graphs presented show that there are many regions where the transport codes are in excellent agreement. However, there are some regions where the results from the three codes differ. The differences in the dose and dose equivalent curves suggest that a follow up study should be performed to determine how ICRP-60 definitions of dose and dose equivalent are being used by the three codes HZETRN, FLUKA and HETC-HEDS. The modeling of the backward neutrons by HZETRN needs to be modified as the current model is placing too much emphasis on backward neutrons at high energies. The cross sections used by the three codes HZETRN, FLUKA and HETC-HEDS are different, and how these differences affect the computed results requires further study. This research also suggests that cross sections used by HZETRN be updated. Future research into a comparison of the results from the HZETRN, HETC-HEDS and FLUKA transport codes for the same shield/target configuration, when exposed to the 1977 solar minimum GCR environment, will aid in trying to isolate causes for the differences between the codes. Results from this study and future comparison studies can provide insight into the HZETRN code operation and bring the code to a high standard of performance so that design engineers can have confidence in its abilities to analyze particle transport associated with a variety of radiation environments.

References

[1] National Aeronautics and Space Administration (NASA), NASA Strategic Plan 2006, Available at www.nasa.gov/pdf/142302main_2006_NASA_Strategic_Plan.pdf.

[2] Wilson, J.W., Tripathi, R.K., Mertens, C.J., Blattnig, S.R., Clowdsley, M.S., Cucinotta, F.A., Tweed, J., Heinbockel, J.H., Walker S.A., & Nealy, J.E., Verification and Validation: High Charge and Energy (HZE) Transport Codes and Future Development, NASA Technical Paper 213784, 2005.

[3] Nealy, J.E., Cucinotta, F.A., Wilson, J.W., Badavi, F.F., Dachev, Ts.P., Tomov, B.T., Walker, S.A., De Angelis G., Blattnig S.R., & Atwell, W., Pre - enineering spaceflight validation of environmental models and the 2005 HZETRN simulation code, Advances in Space Research 40, 1593-1610, 2007.

[4] Wilson, J.W., Badavi, F.F., Cucinotta, F.A., Shinn, J.L., Badhwar, G.D., Silberberg, R., Tsao, C.H., Townsend L.W., & Tripathi, R.K., HZETRN: Description of a Free - Space Ion and Nucleon Transport and Shielding Computer Program, NASA Technical Paper 3495, 1995.

[5] Cucinotta, F.A., Wilson, J.W., Saganti, P., Hu, X., Kim, M.Y., Cleghorn, T., Zeitlin C., & Tripathi, R.K., Isotopic dependence of GCR fluence behind shielding, Radiation Measurements 41, 1235-1249, 2006.

[6] Slaba, T.C., Blattnig, S.R., Walker, S.A., Wilson, J.W., & Badavi, F.F., An Improved Neutron Transport Algorithm for HZETRN, 37th COSPAR conference, Montreal, Canada, 2008.

[7] Slaba, T.C., Heinbockel J.H., & Blattnig, S.R., Neutron Transport Models and Methods for HZETRN and coupling to Low Energy Light Ion Transport, Society of Automative Engineers (SAE) International Conference on Environmental Systems (ICES), 2008. Available at http://www.sae.org/technical/papers/2008-01-2162.

[8] Wilson, J.W., Tripathi, R.K., Badavi, F.F., & Cucinotta, F.A., Standardized Radiation Shield Design Method: 2005 HZETRN, Society of Automative Engineers (SAE) International Conference on Environmental Systems (ICES), 2006. Available at http://www.sae.org/technical/papers/2006-01-2109.

[9] Webber, W.R., An Evaluation of the Radiation Hazard Due to Solar Particle Events, Boeing Report D2-90469, AeroSpace Division, The Boeing Company, 1963.

[10] Quenby J.J., & Webber, W.R., Cosmic Ray Cut Off Rigidities and the Earth's Magnetic Field, Philosophical Magazine 4, 90-112, 1959.

[11] Gabriel, T.A., Bishop, B.L., Alsmiller, F.S., Alsmiller, R.G., & Johnson, J.O., CALOR95: A Monte Carlo Program Package for the Design and Analysis of Calorimeter Systems, Oak Ridge National Laboratory Technical Memorandum 11185, 1995.

[12] Townsend, L.W., Miller, T.M., & Gabriel, T.A., HETC Radiation Transport Code Development for Cosmic Ray Shielding Applications in Space, Radiation Protection Dosimetry 115, 135-139, 2005.

[13] Fasso, A., Ferrari, A., Ranft, J., & Sala, P.R., FLUKA: a multi-particle transport code, CERN-2005-10, INFN/TC 05/11, SLAC-R-773, 2005.

[14] Battistoni, G., Muraro, S., Sala, P.R., Cerutti, F., Ferrari, A., Roesler, S., Fasso, A., & Ranft, J., The FLUKA code: Description and benchmarking, Proceedings of the Hadronic Shower Simulation Workshop 2006, Fermilab 6 - 8 September 2006, Albrow, M., & Raja R., eds., American Institute of Physics Conference Proceeding 896, 31-49, 2007.

[15] Wilson, J.W., Townsend, L.W., Schimmerling, W., Khandelwal, G.S., Khan, F., Nealy, J.E., Cucinotta, F.A., Simonsen, L.C., Shinn, J.L., & Norbury, J.W., Transport Methods and Interactions for Space Radiations, NASA Research Publication 1257, 1991.

[16] Shinn, J.L., Wilson, J.W., Weyland, M., & Cucinotta, F.A., Improvements in Computational Accuracy of BRYNTRN (A Baryon Transport Code), NASA Technical Paper 3093, 1991.

[17] Wilson, J.W., & F. F. Badavi, F.F., Methods of Galactic Heavy Ion Transport, Radiation Research 108, 231-237, 1986.

[18] Wilson, J.W., Analysis of the Theory of High - Energy Ion Transport, NASA Technical Note D-8381, 1977.

[19] Clowdsley, M.S., Wilson, J.W., Heinbockel, J.H., Tripathi, R.K., Singleterry R.C., & Shinn, J.L., An Improved Elastic and Nonelastic Neutron Transport Algorithm for Space Radiation, NASA Technical Paper 210299, 2000.

[20] Clowdsley, M.S., Heinbockel, J.H., Kaneko, H., Wilson, J.W., Singleterry R.C., & Shinn, J.L., A Comparison of the Multigroup and Collocation Methods for Solving the Low Energy Neutron Boltzmann Equation, Canadian Journal of Physics 78, 45-56, 2000.

[21] Feldman, G.A., A Forward - Backward Fluence Model for the Low Energy Neutron Boltzmann Equation, Ph. D. Thesis, Old Dominion University, Norfolk, Virginia, 2003.

[22] Slaba, T.C., Heinbockel, J.H., Wilson, J.W., Blattnig, S.R., Clowdsley, M.S., & Badavi, F.F., A New Method for Calculating Low Energy Neutron Flux, SAE ICES - 01 - 2149, 2006. Society of Automative Engineers (SAE) International Conference on Environmental Systems (ICES), 2006. Available at http://www.sae.org/technical/papers/2006-01-2149.

[23] Slaba, T.C., Three Methods for Solving the Low Energy Neutron Boltzmann Equation, Ph. D. Thesis, Old Dominion University, Norfolk, Virginia, 2007.

[24] Heinbockel, J.H., Slaba, T.C., Wilson, J.W., Blattnig, S.R., Clowdsley, M.S., & Badavi, F.F., Comparison of Numerical Solution Techniques for Calculating Low Energy Neutrons, Society of Automative Engineers (SAE) International Conference on Environmental Systems (ICES), 2007. Available at http://www.sae.org/technical/papers/2007-01-3117.

[25] National Council on Radiation Protection and Measurements (NCRP), Conceptual Basis for Calculations of Absorbed Dose Distributions, NCRP Report 108, 1995.

[26] National Council on Radiation Protection and Measurements (NCRP), Radiation Protection Guidance for Activities in Low - Earth Orbit, NCRP Report 132, 2000.

[27] National Council on Radiation Protection and Measurements (NCRP), Operational Radiation Safety Program for Astronauts in Low - Earth Orbit: A Basic Framework, NCRP Report 142, 2002.

[28] Ingersoll, D.T., Roussin, R.W., Fu, C.Y., & White, J.E., DABL69: A broad group neutron / photon cross section library for defense nuclear applications, Oak Ridge National Laboratory Technical Memorandum 10568, 1988.

[29] International Commission on Radiological Protection (ICRP), The 1990 Recommendations of the International Commission on Radiological Protection, ICRP Publication 60, Annals of ICRP 21 (1-3), 1991.
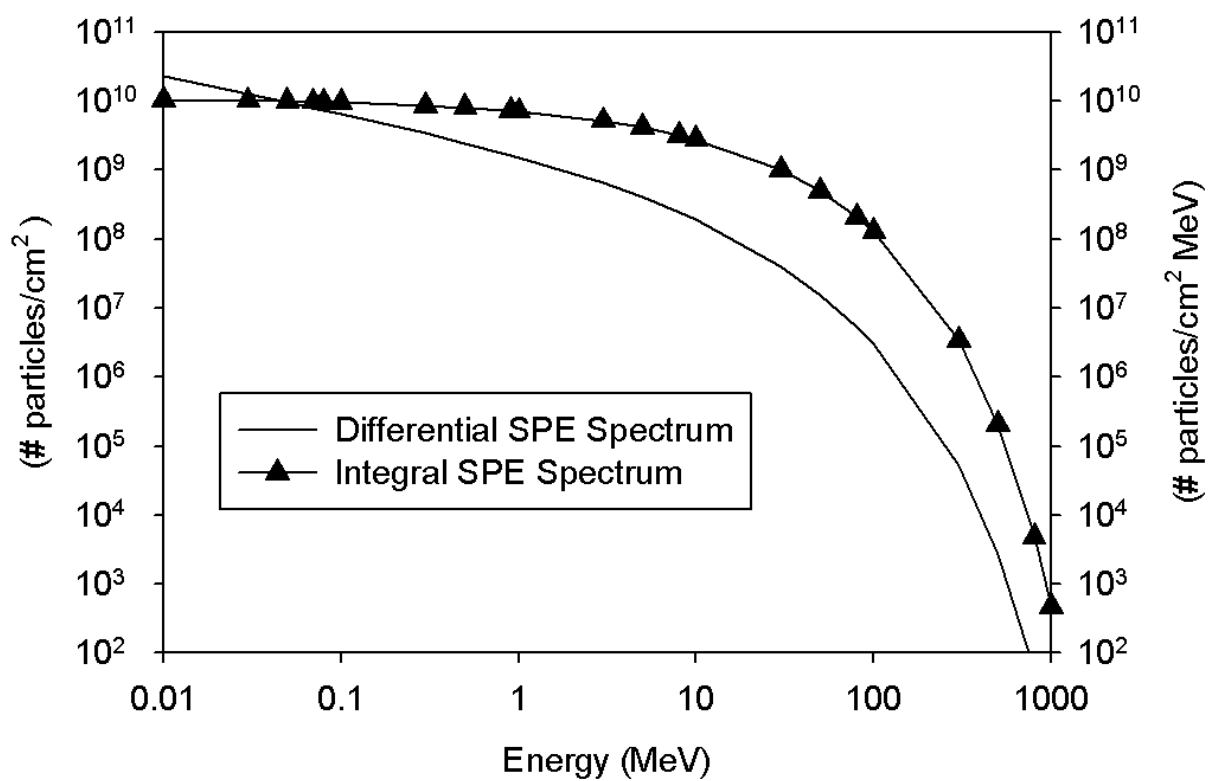
Figure 1: Webber 1956 integral and differential SPE spectrum with 100 MV rigidity. The integral spectrum vertical axis is on the left and the differential spectrum vertical axis is on the right.
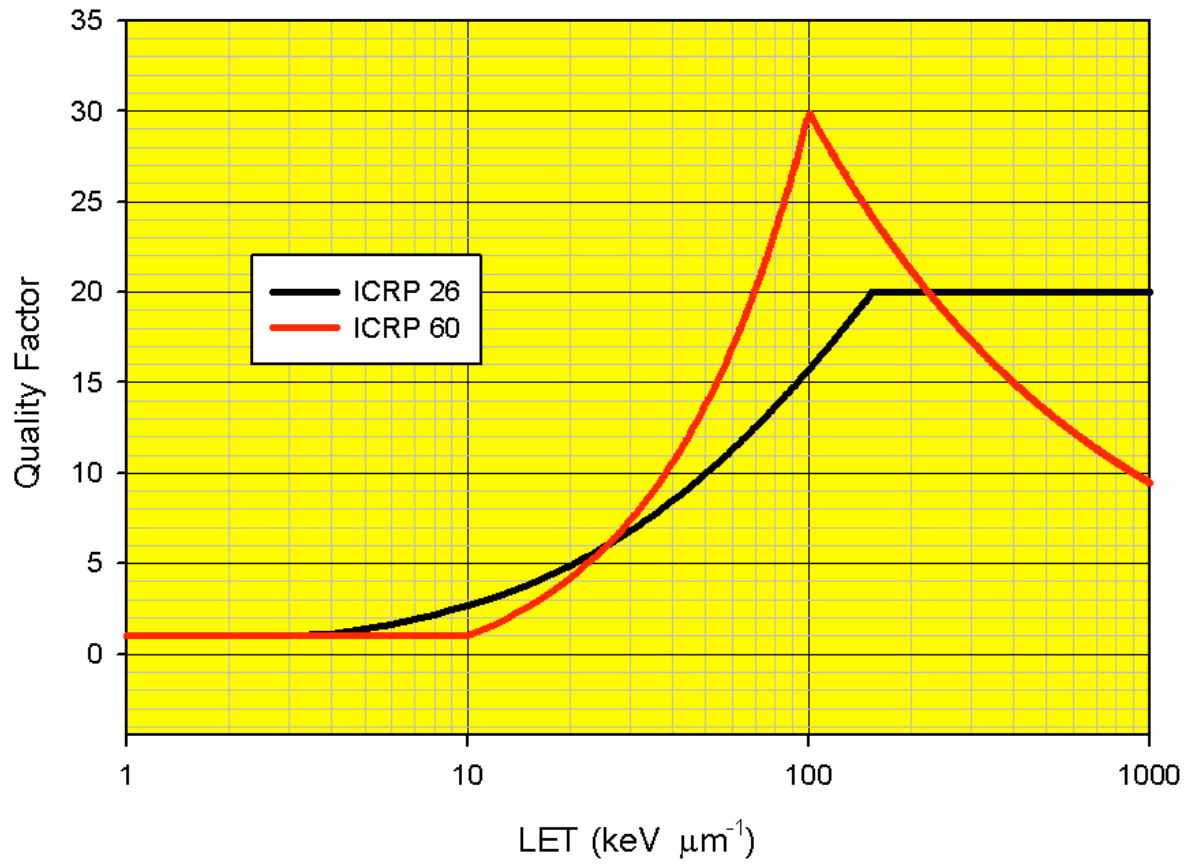
Figure 2: $Q(L)$ as defined by equation (19).
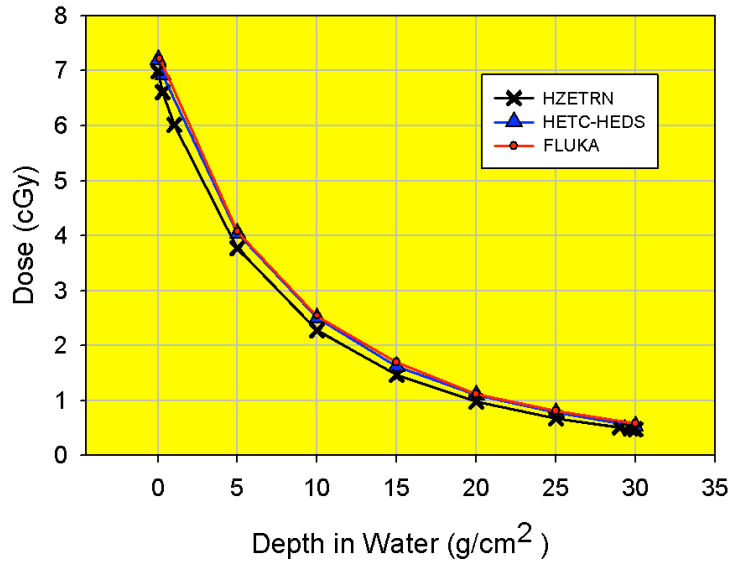
Figure 3: Dose versus depth in water after aluminum shield.
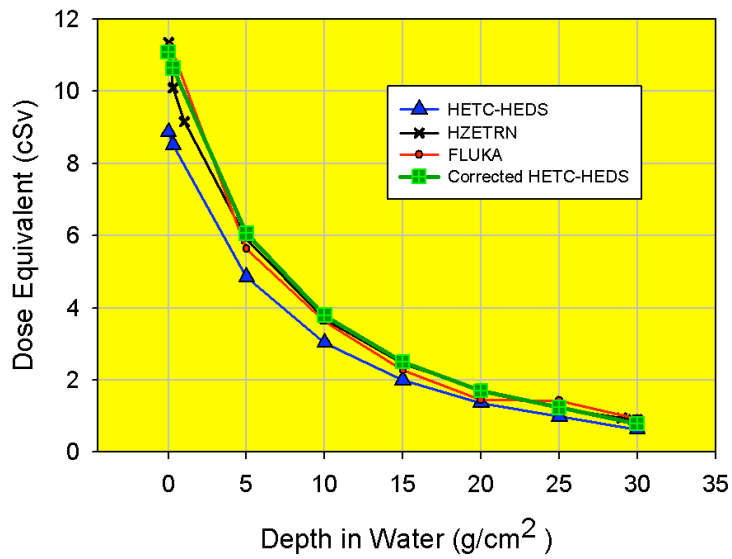
Figure 4: Dose equivalent versus depth in water after aluminum shield.
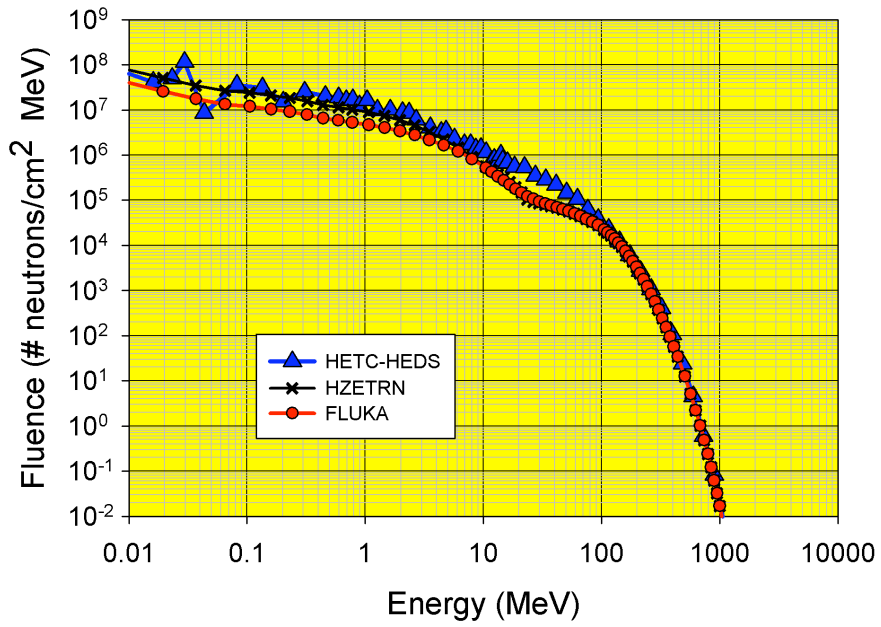
Figure 5: Forward neutron fluence versus energy. Water depth is 0 g/cm^2.
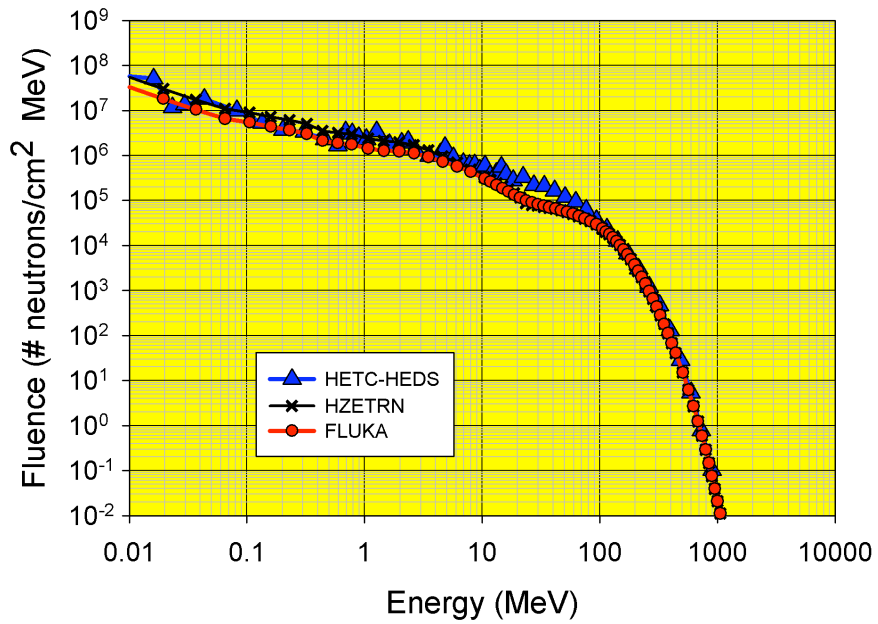
Figure 6: Forward neutron fluence versus energy. Water depth is 10 g/cm^2.
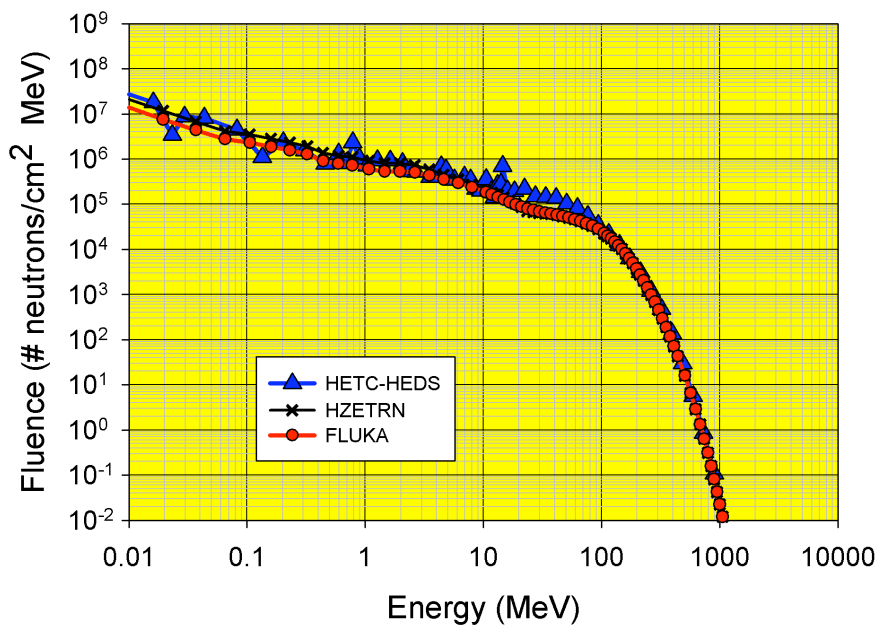
Figure 7: Forward neutron fluence versus energy. Water depth is 20 g/cm^2.
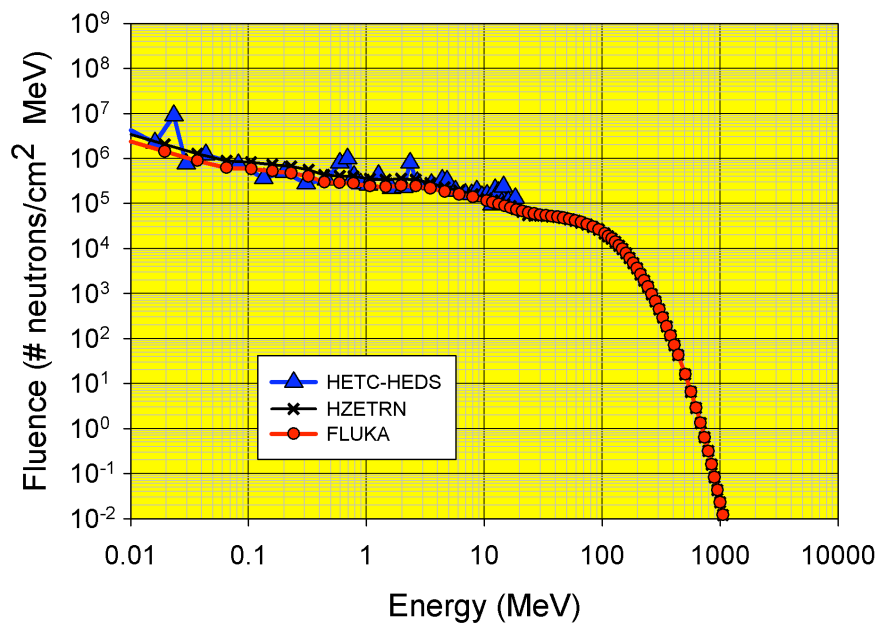
Figure 8: Forward neutron fluence versus energy. Water depth is 30 g/cm^2.
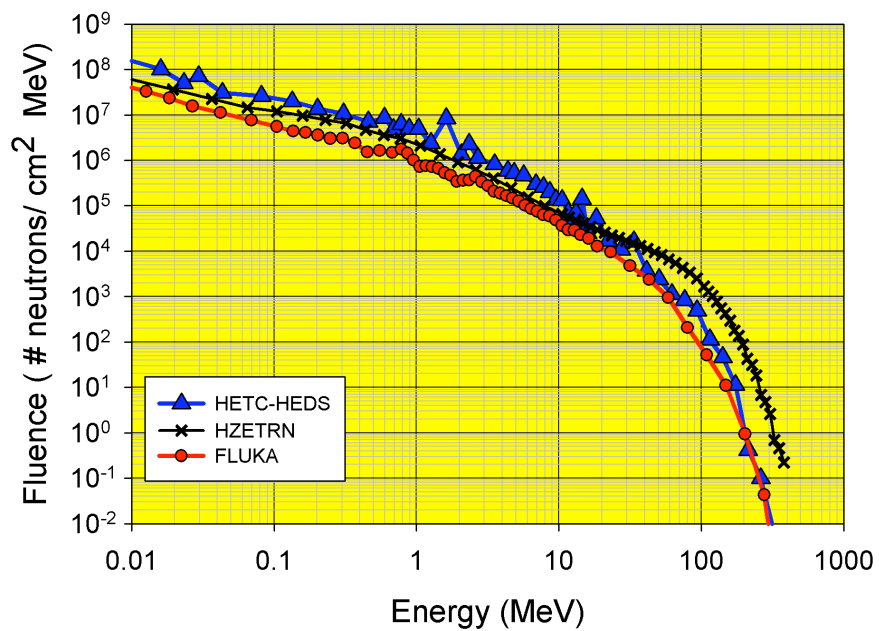
Figure 9: Backward neutron fluence versus energy. Water depth is 0 g/cm^2.
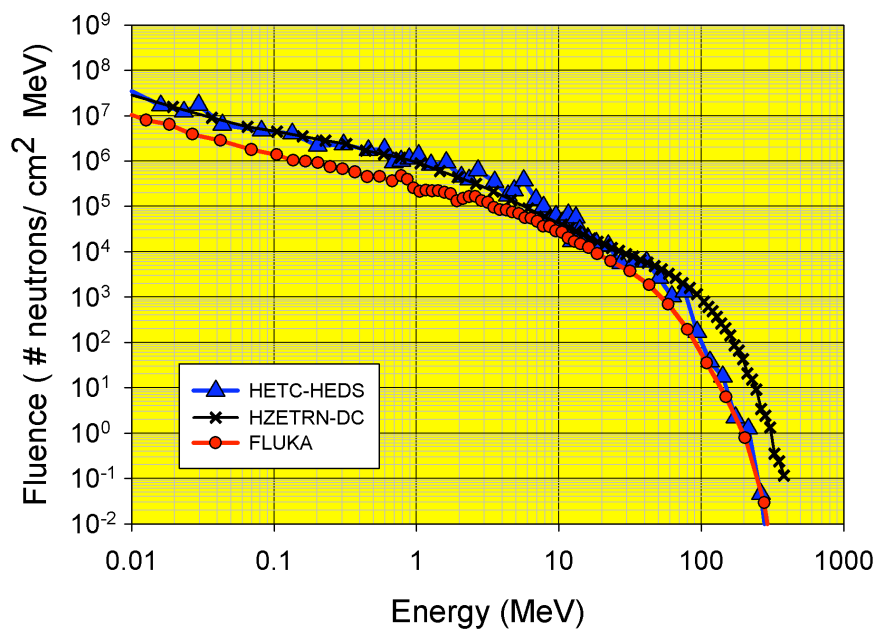
Figure 10: Backward neutron fluence versus energy. Water depth is 10 g/cm^2.
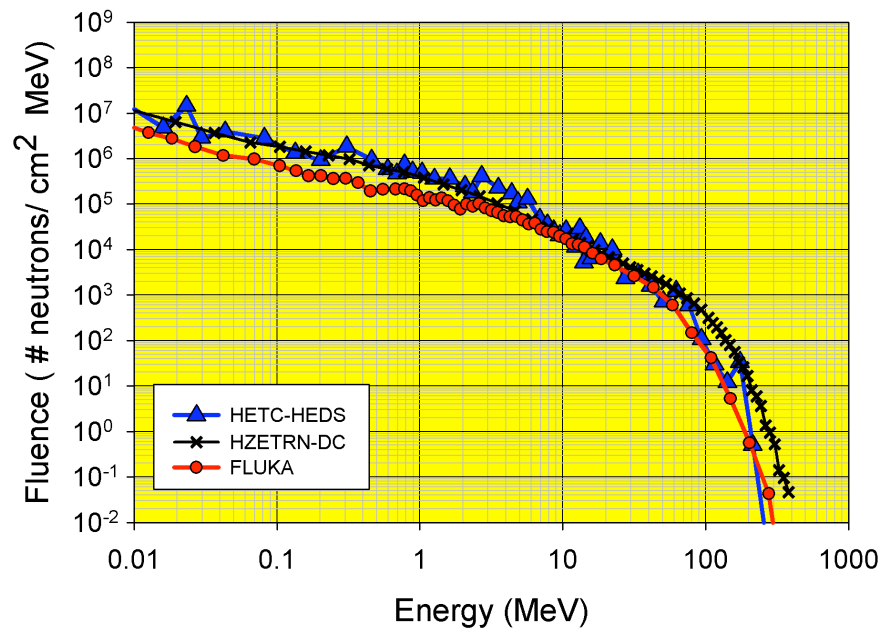
Figure 11: Backward neutron fluence versus energy. Water depth is 20 g/cm^2.
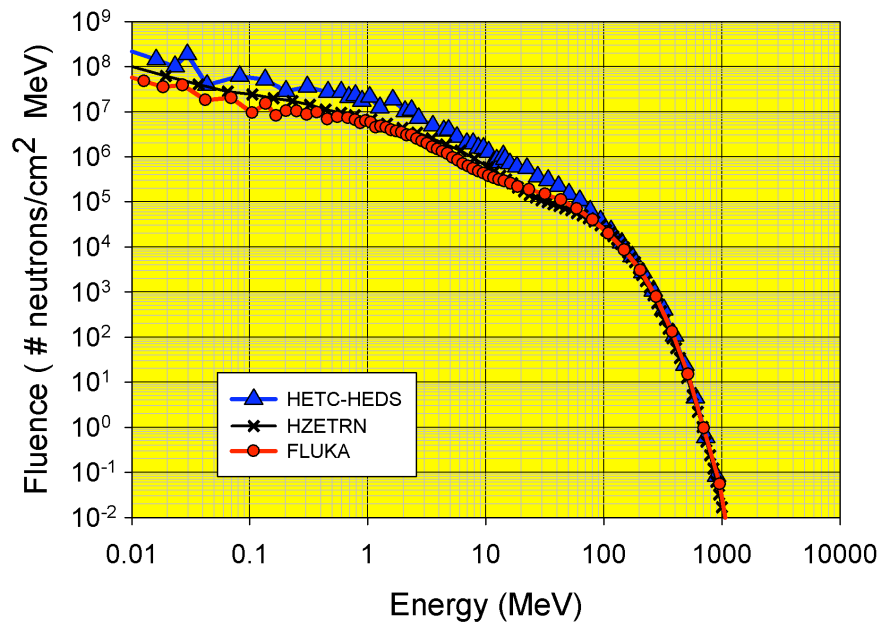
Figure 12: Total neutron fluence versus energy. Water depth is 0 g/cm^2.
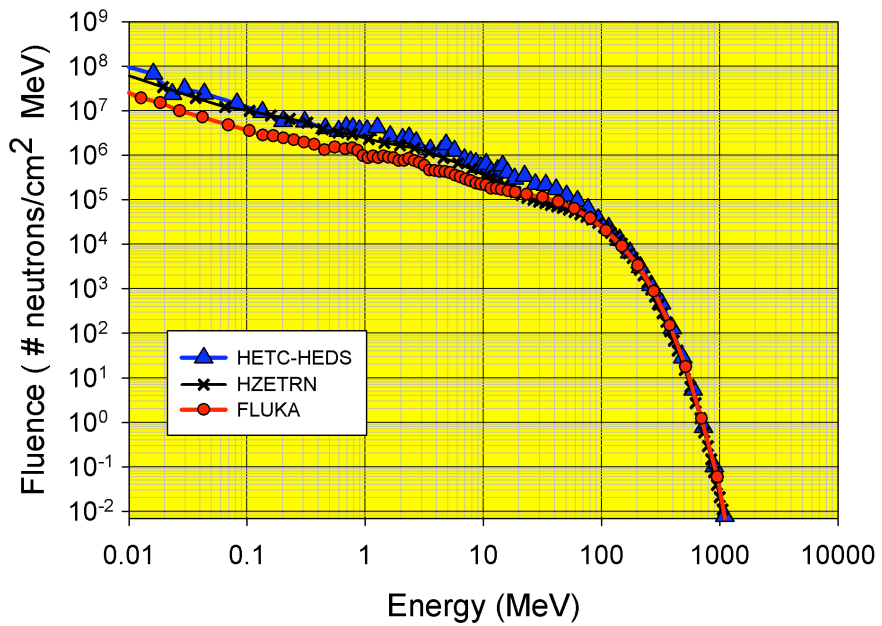
Figure 13: Total neutron fluence versus energy. Water depth is 10 g/cm^2.
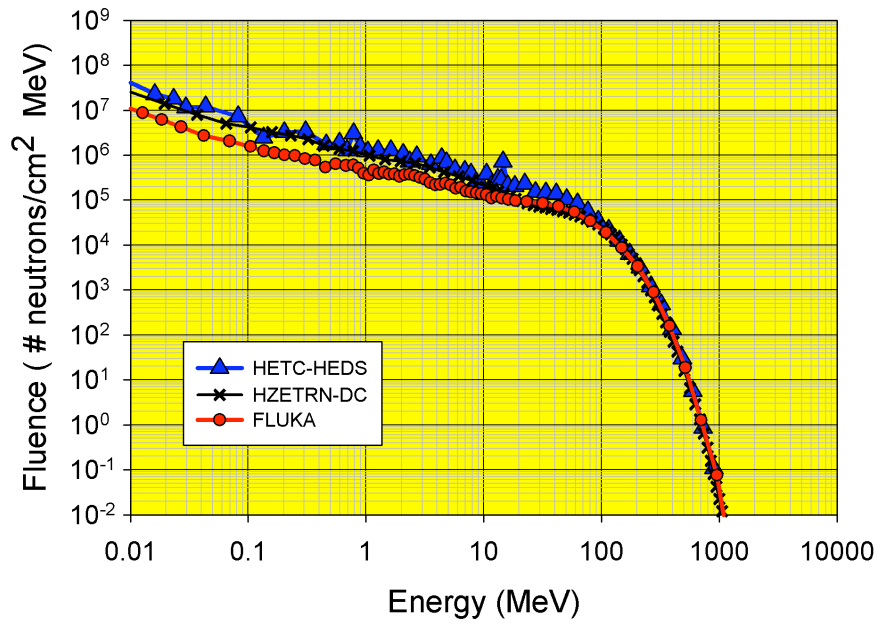
Figure 14: Total neutron fluence versus energy. Water depth is 20 g/cm^2.
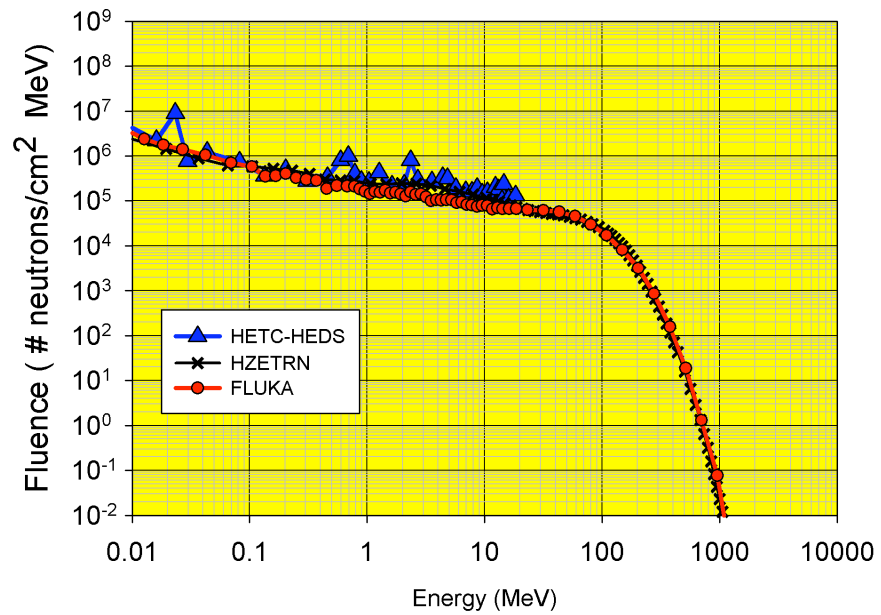
Figure 15: Total neutron fluence versus energy. Water depth is 30 g/cm^2.

23
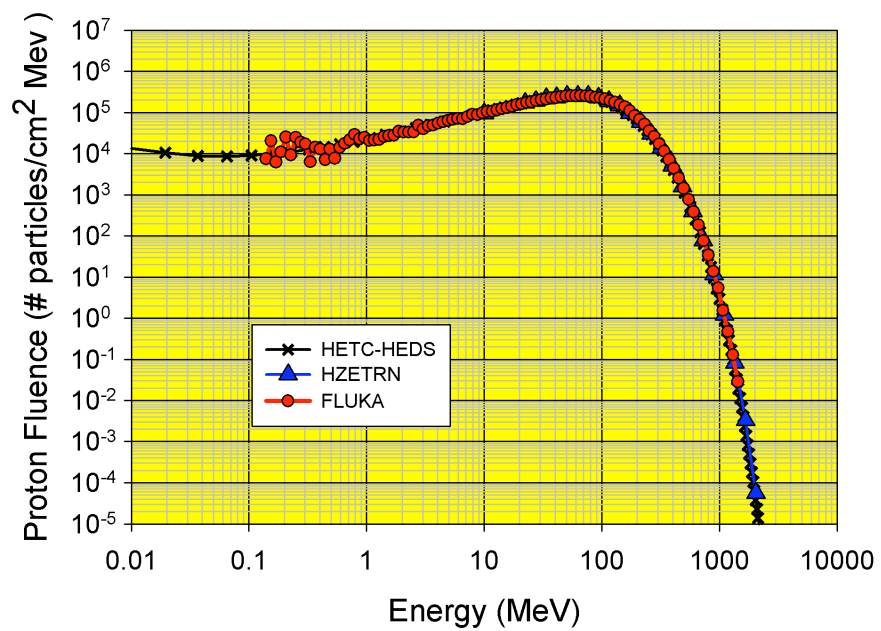
Figure 16: Total proton fluence versus energy. Water depth is 0 g/cm^2.
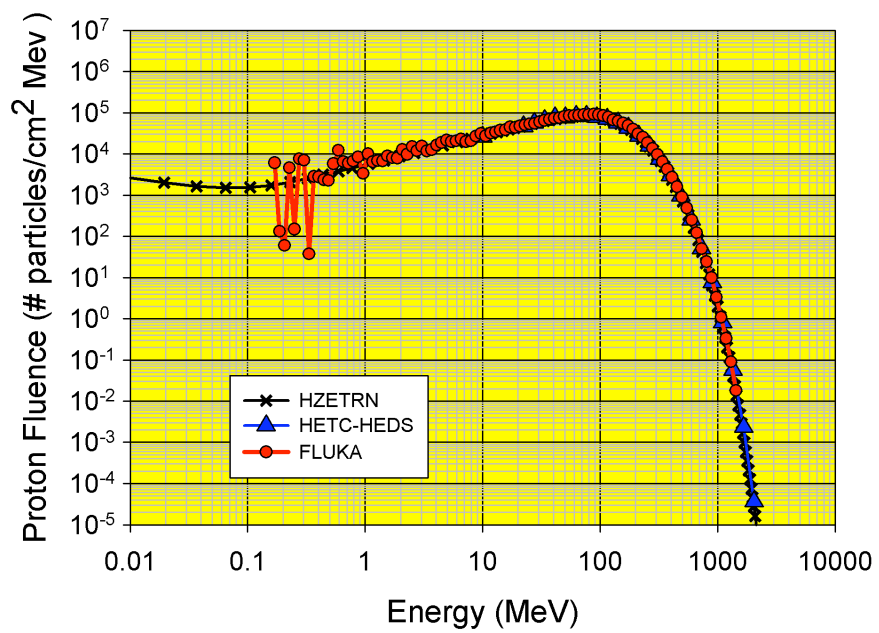
Figure 17: Total proton fluence versus energy. Water depth is 10 g/cm^2.

24
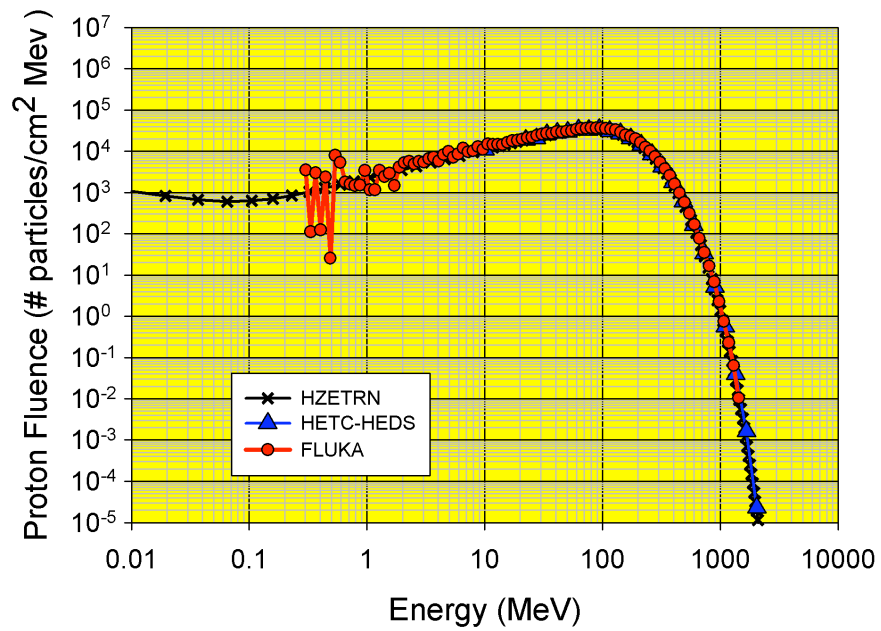
Figure 18: Total proton fluence versus energy. Water depth is 20 g/cm^2.
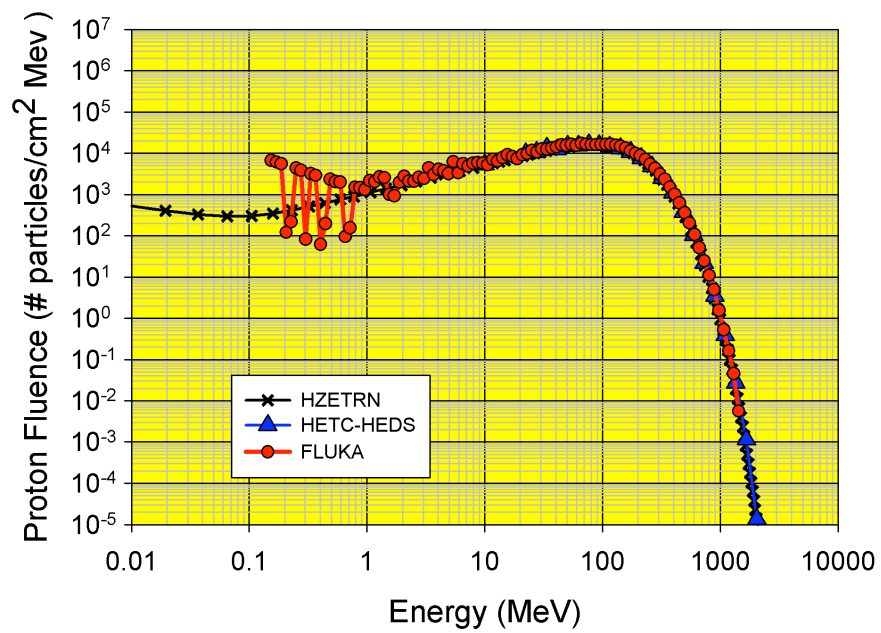
Figure 19: Total proton fluence versus energy. Water depth is 30 g/cm^2.

25
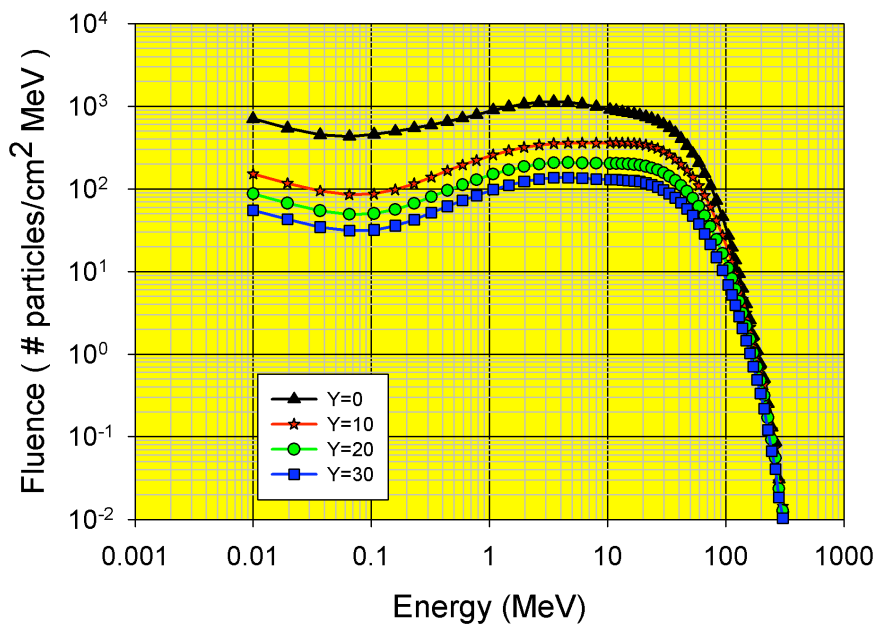
Figure 20: HZETRN total ^{2}H fluence versus energy. Water depth is Y (g/cm^2).
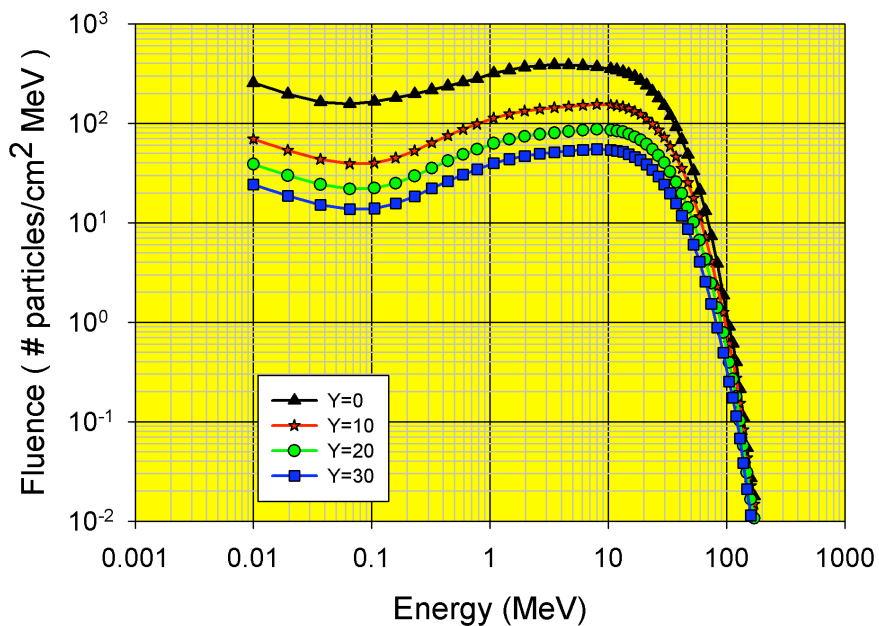
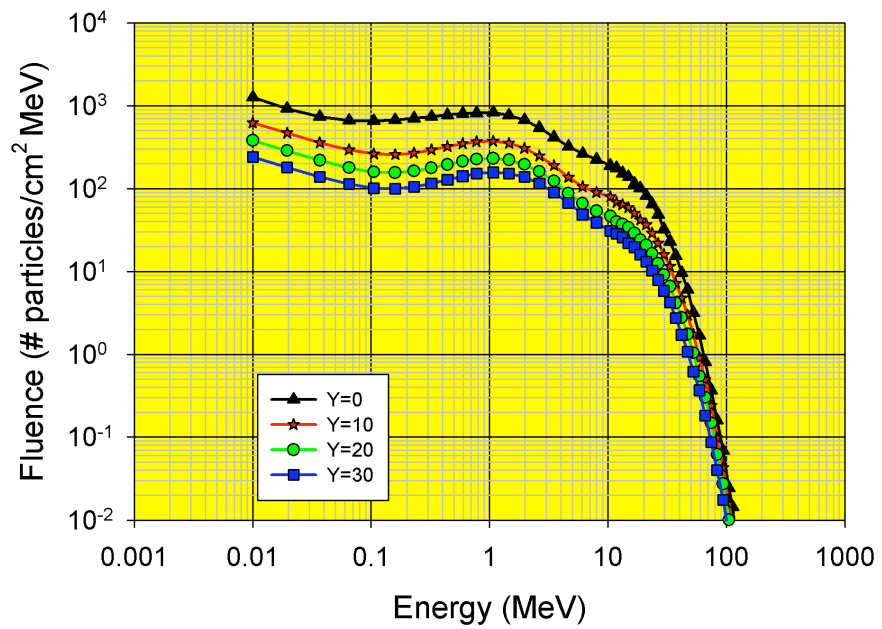Figure 21: HZETRN total ^{3}H fluence versus energy. Water depth is Y (g/cm^2).

26
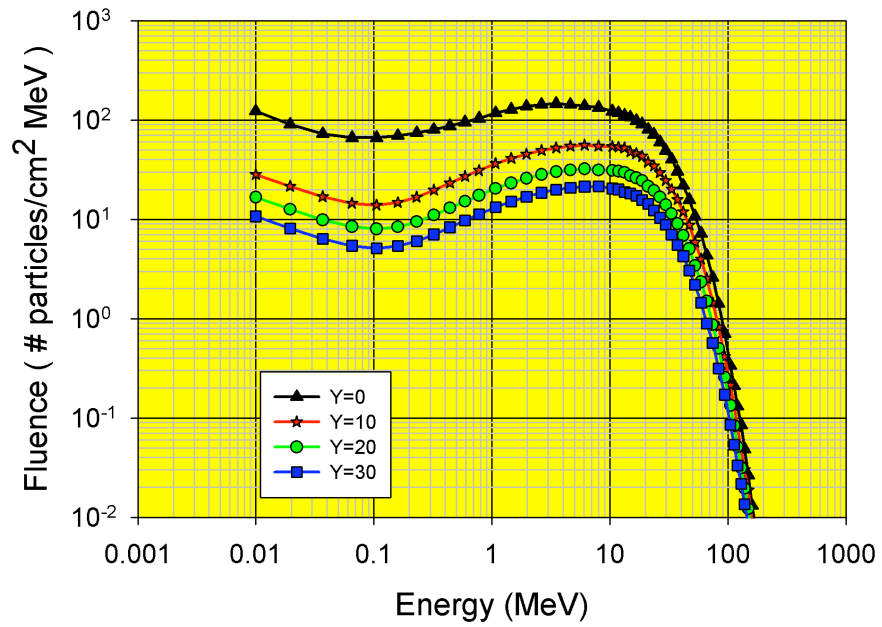
Figure 22: HZETRN total ^{3}He fluence versus energy. Water depth is Y (g/cm^2).

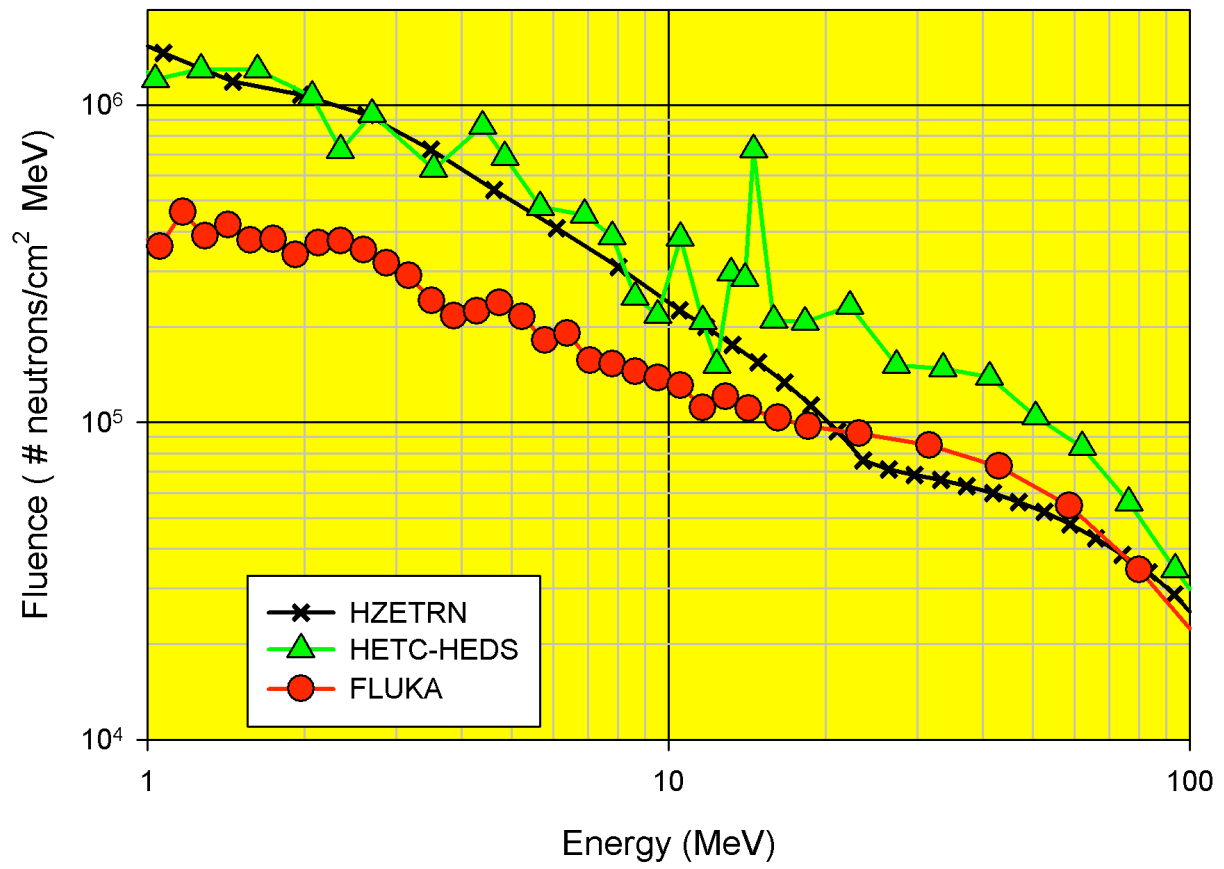Figure 23: HZETRN total ^{4}He fluence versus energy. Water depth is Y (g/cm^2).

27

Figure 24: Enlargement of Figure 15.

REPORT DOCUMENTATION PAGE

1. REPORT DATE *(DD-MM-YYYY)*	2. REPORT TYPE	3. DATES COVERED *(From - To)*
01-01-2009	Technical Publication	

4. TITLE AND SUBTITLE

Comparison of Radiation Transport Codes, HZETRN, HETC and FLUKA, Using the 1956 Webber SPE Spectrum

5a. CONTRACT NUMBER

5b. GRANT NUMBER

5c. PROGRAM ELEMENT NUMBER

6. AUTHOR(S)

Heinbockel, John H.; Slaba, Tony C.; Blattnig, Steve R.; Tripathi, Ram K.; Townsend, Lawrence W.; Handler, Thomas; Gabriel, Tony A.; Pinsky, Lawrence S.; Reddell, Brandon; Clowdsley, Martha S.; Singleterry, Robert C.; Norbury, John W.; Badavi, Francis F.; Aghara, Sukesh K.

5d. PROJECT NUMBER

5e. TASK NUMBER

5f. WORK UNIT NUMBER

651549.02.07.01

7. PERFORMING ORGANIZATION NAME(S) AND ADDRESS(ES)

NASA Langley Research Center
Hampton, VA 23681-2199

8. PERFORMING ORGANIZATION REPORT NUMBER

L-19555

9. SPONSORING/MONITORING AGENCY NAME(S) AND ADDRESS(ES)

National Aeronautics and Space Administration
Washington, DC 20546-0001

10. SPONSOR/MONITOR'S ACRONYM(S)

NASA

11. SPONSOR/MONITOR'S REPORT NUMBER(S)

NASA/TP-2009-215560

12. DISTRIBUTION/AVAILABILITY STATEMENT

Unclassified - Unlimited
Subject Category 93
Availability: NASA CASI (443) 757-5802

13. SUPPLEMENTARY NOTES

14. ABSTRACT

Protection of astronauts and instrumentation from galactic cosmic rays (GCR) and solar particle events (SPE) in the harsh environment of space is of prime importance in the design of personal shielding, spacecraft, and mission planning. Early entry of radiation constraints into the design process enables optimal shielding strategies, but demands efficient and accurate tools that can be used by design engineers in every phase of an evolving space project. The radiation transport code, HZETRN, is an efficient tool for analyzing the shielding effectiveness of materials exposed to space radiation. In this paper, HZETRN is compared to the Monte Carlo codes HETC-HEDS and FLUKA, for a shield/target configuration comprised of a 20 g/cm^2 Aluminum slab in front of a 30 g/cm^2 slab of water exposed to the February 1956 SPE, as modeled by the Webber spectrum. Neutron and proton fluence spectra, as well as dose and dose equivalent values, are compared at various depths in the water target. This study shows that there are many regions where HZETRN agrees with both HETC-HEDS and FLUKA for this shield/target configuration and the SPE environment. However, there are also regions where there are appreciable differences between the three computer codes.

15. SUBJECT TERMS

Space radiation; Raditation transport; Shielding

16. SECURITY CLASSIFICATION OF:			17. LIMITATION OF ABSTRACT	18. NUMBER OF PAGES	19a. NAME OF RESPONSIBLE PERSON
a. REPORT	b. ABSTRACT	c. THIS PAGE			STI Help Desk (email: help@sti.nasa.gov)
U	U	U	UU	35	19b. TELEPHONE NUMBER *(Include area code)* (443) 757-5802